INFLUENCE OF INITIAL POROSITY ON STRENGTH PROPERTIES OF S235JR STEEL AT LOW STRESS TRIAXIALITY

P.G. KOSSAKOWSKI[1]

The paper discusses the influence of the initial parameters on the strength parameters of S235JR steel at low stress triaxiality. The analysis was performed using the Gurson-Tvergaard-Needleman (GTN) material model, which takes into consideration the material structure. The initial material porosity was defined as the void volume fraction f_0. The fully dense material without pores was assumed and the typical and maximum values of porosity were considered for S235JR steel in order to analyse the porosity effect. The strength analysis of S235JR steel was performed basing on the force-elongation curves obtained experimentally and during numerical simulations. Taking into consideration the results obtained, the average values of the initial void volume fraction $f_0 = 0.001$ for S235JR steel is recommended to use in a common engineering calculations for elements operating at low stress triaxiality. In order to obtain more conservative results, the maximum values of $f_0 = 0.0024$ may be used.

Key words: S235JR steel, Gurson-Tvergaard-Needleman material model, GTN, porosity, numerical simulations.

1. INTRODUCTION

The failure process of most metals and alloys, including the structural steel grades commonly used in the technique, is strongly connected to the material microstructure, especially with the microstructural defects. Micro-defects in the form of voids occurs on the inclusions and second-phase particles existing in the material.

There are several basic types of the failure mechanisms, i.e. plastic, cleavage and brittle intergranular, shear or void-sheeting and ductile fracture [1]. In the processes of shear and ductile fracture, the failure of the material is attributable to the nucleation, growth and coalescence of voids (Fig. 1 and 2). The growth and coalescence of voids result in the development of localised plastic deformations, which have the greatest impact on the material failure.

---

[1] Strength of Materials and Concrete Structures, Faculty of Civil and Environmental Engineering, Kielce University of Technology, Al. Tysiąclecia Państwa Polskiego 7, 25-314 Kielce, Poland, e-mail: kossak@tu.kielce.pl
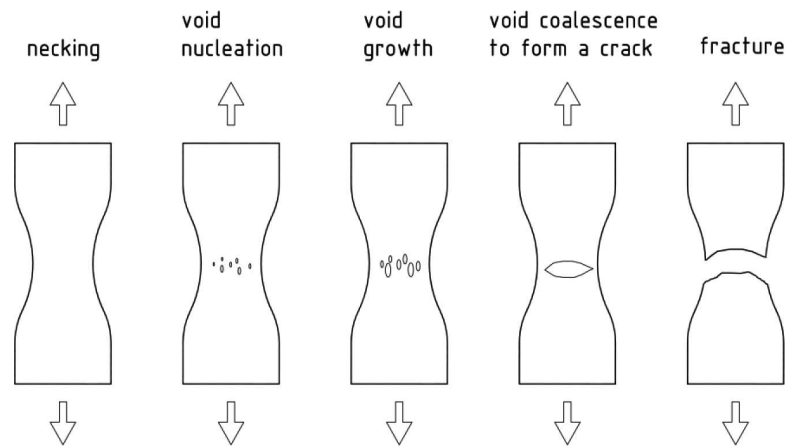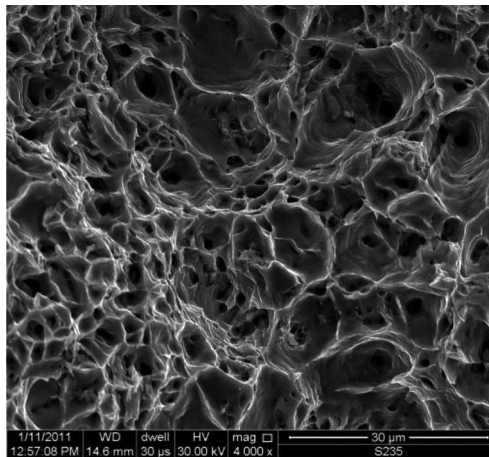
Fig. 1. Micro-mechanism of ductile fracture.

Fig. 2. Ductile fracture area of S235JR steel.

An analysis of the above phenomena is impossible using a classical theory based on the continuum mechanics of the materials. It is necessary to use the damage material models taking into account the influence of the microstructural defects on the material strength by defining the relationship between the particular failure stages and the strength of the material. The one of such damage material models was Gurson model [2] for a porous solid, defining in a modified Huber-Mises-Hencky criterion the influence of an increase in the void volume fraction on the strength of the material. The original Gurson model was modified by Tvergaard [3] who introduced selected microstructural parameters and plastic properties of a material to the criterion.

In this modified form it is referred as Gurson-Tvergaard-Needleman (GTN) material model [4].

The GTN material model is one of a basic models used in the strength analysis of many materials commonly used in a broadly defined engineering. According to the current standards obligatory in European Union, for instance [5] and its commentary by Sedlacek et al. [6], the GTN material model is recommended to use in the analysis of pre-failure condition for building structures. The GTN model ensures good consistency of the results obtained numerically and experimentally in opposition to the models based on HMH criterion, which is shown in several studies, eg. [7, 8].

Although the GTN model in a modified form was developed in the 80s of last century, it is still the subject of many studies, e.g. [9], and many related features need to be solved. The general drawback is the lack of standardised microstructural parameters to apply GTN model for steels used most commonly in civil engineering. Another problem is the size effect encountered during numerical simulations with GTN model, which reveals the softening of the final part of the strength curve. The computational procedure, which allows to estimate numerically the limit load capacity and simulate the failure, needs to be elaborated also in order to perform common engineering calculations of structural elements operating in the nonlinear ranges.

The catastrophic failures of engineered structures, which recently took place in Poland, incline to deal with the topic related with the analysis of the pre-failure condition and estimation of the limit loads beyond the elastic range. Several authors engage the issues related to estimation of the load-bearing capacity of the structures [10, 11] and the stability of the elements [12-14] as well as the development of the methods used for the damage detection [15, 16]. The GTN material model seems to be very useful in the strength analyses and may be applied in common engineering practise. Therefore a wide research program was focused to elaborate procedures which enable to estimate numerically the load-bearing capacity of steel building construction elements made of S235JR steel operating in pre-failure states. The method is based on the modified GTN material model taking into account the impact of the microdamage. The results will be helpful in the analysis, and in the expert opinions on the load-bearing capacity of steel components and structures, because S235JR steel is the main steel grade used in civil engineering.

Taking into account the problems described above, especially the lack of microstructural parameters for steels used most commonly in civil engineering, one of the main part of the research program is to standardise the material parameters of the GTN model for S235JR steel. In this study the first parameter of the GTN material model, such as porosity corresponding to the initial void volume fraction (*VVF*) f_0, was analysed for S235JR steel and the influence of porosity on strength of the material was examined. The fully dense material without pores was assumed and the typical and maximum values of porosity were assumed for S235JR steel in order to analyse the porosity effect.

The analysis was performed for the tensile elements at low stress state, defined by initial stress triaxiality $\sigma_m/\sigma_e = 1/3$, where σ_m and σ_e denotes mean and effective stress, respectively.

The presented results may be used for the analysis and the expertises connected with the assessment of the load-carrying capacity and safety of the structural elements made of S235JR steel performed using the GTN material model. It seems that phenomena observed for S235JR steel may occur in another steel grades with similar porosity and metallurgical composition.

2. Gurson-Tvergaard-Needleman (GTN) damage material model

The first model to take into consideration microdamage was the Gurson model [2], which assumed that the proportion of voids in the plastic potential function was dependent on the void volume fraction f. The original Gurson condition was later modified by Tvergaard and Needleman [3, 4]. The modified GTN plastic potential function is described as:

$$(2.1) \qquad \Phi = \left(\frac{\sigma_e}{\sigma_0}\right)^2 + 2q_1 f^* \cosh\left(q_2 \frac{3\sigma_m}{2\sigma_0}\right) - \left(1 + q_3 f^{*2}\right) = 0$$

where: σ_e – effective stress according to the HMH hypothesis, σ_0 – yield stress of the material, σ_m – hydrostatic pressure (mean stress), f^* – actual void volume fraction, q_i –Tvergaard's coefficients describing the plastic properties of the material.

In the GTN model, the actual void volume fraction f^* is defined as:

$$(2.2) \qquad f^* = \begin{cases} f & \text{for} \quad f \leq f_c \\ f_c + \dfrac{\bar{f}_F - f_c}{f_F - f_c}(f - f_c) & \text{for} \quad f_c < f < f_F \\ \bar{f}_F & \text{for} \quad f \geq f_F \end{cases}$$

where: f_c – critical void volume fraction at which the void coalescence starts, f_F – void volume fraction corresponding to the complete loss of the material strength, at final separation of the material, $\bar{f}_F = \left(q_1 + \sqrt{q_1^2 - q_3}\right)/q_3$.

An increase in the void volume fraction $\dot{f}$ is defined by relationship:

$$(2.3) \qquad \dot{f} = \dot{f}_{gr} + \dot{f}_{nucl} = (1 - f)\,\dot{\varepsilon}^{pl} : \mathbf{I} + \frac{f_N}{s_N \sqrt{2\pi}} \exp\left[-\frac{1}{2}\left(\frac{\varepsilon^{pl}_{e\,m} - \varepsilon_N}{s_N}\right)^2\right] \cdot \dot{\varepsilon}^{pl}_{e\,m}$$

where: $\dot{f}_{gr}$ – change due to growth of voids existing in the material, $\dot{f}_{nucl}$ – change due to nucleation of new voids, f_N – volume fraction of nucleated voids, s_N – standard deviation of nucleation strain, $\dot{\varepsilon}^{pl}$ – plastic strain rate tensor, $\mathbf{I}$ – second-order unit tensor, ε_N – mean strain of the void nucleation, $\varepsilon^{pl}_{e\,m}$ – equivalent plastic strain in the matrix material, $\dot{\varepsilon}^{pl}_{e\,m}$– equivalent plastic strain rate in the matrix material.

3. Initial void volume fraction f_0 for S235JR steel

The initial void volume fraction was assumed for two general situations. On the one hand the fully dense material without pores was considered, on the other hand the typical and maximum values of porosity were assumed for S235JR steel.

As mentioned above, in the first situation, for the material without pores the initial void volume fraction was assumed as $f_0 = 0$.

In order to determine typical values of initial porosity for S235JR steel, the microstructural examinations were performed. To this end the microstructural images of S235JR steel with a ferritic-perlitic matrix (Fig. 3) were obtained. A large number of non-metallic inclusions, mainly sulfides and brittle oxides was reported.
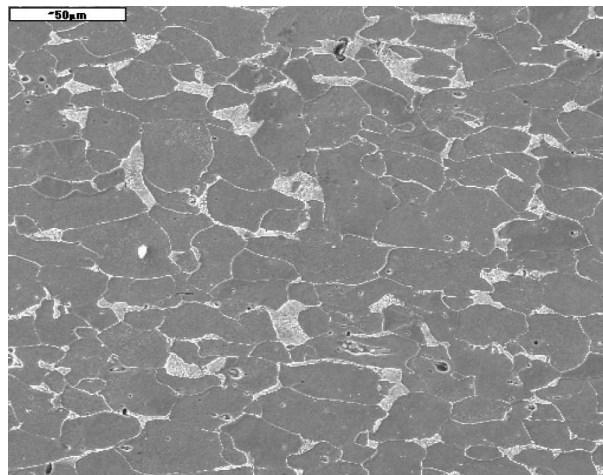

Fig. 3. SEM image of S235JR steel.

Sulfide inclusions were elongated in shape, and their distribution in the volume was irregular, they were arranged in bands. In the tested material other non-metallic inclusions were found, the uniaxial brittle oxides. They occured together with sulfide inclusions. The basic stereological parameters were determined to fully characterize the non-metallic inclusions in the material.

The values of initial void volume fraction for S235JR steel ranged for different parts in longitudinal and central cross-sections. Considering values obtained, the average initial void volume fraction for S235JR steel was determined as $f_0 = 0.001$.

In order to determine the maximum value of the initial porosity for S235JR steel, it was considered, that the material contains the non-metallic inclusions of sulphur and manganese. Assuming a spherical shape of the inclusions, the initial void volume fraction can be estimated using Franklin's formulae [17]:

$$(3.1) \qquad f_0 = 0.054 \left(S\% - \frac{0.001}{Mn\%} \right)$$

where: S, Mn – proportional content of sulphur and manganese inclusions in a material.

According to the metallurgical requirements given in [18] the maximum content of sulphur and manganese for S235JR steel is $Mn = 1.3\%$ i $S = 0.045\%$. In results, the maximum initial void volume fraction estimated for S235JR steel using formulae (3.1) is equal $f_0 = 0.0024$.

4. GTN MATERIAL PARAMETERS FOR S235JR STEEL

The other material parameters for S235JR steel were established basing on the results of experiments and numerical simulations reported in [19].

In the first step the standard static tensile strength tests were performed, according to [20]. The specimens with a circular cross-section of nominal diameter $d = 10$ mm, the length of the measuring base $l_0 = 50$ mm, and the primary cross-sectional area $S_0 = 78.5$ mm^2 were used. The average strength parameters obtained during the tests were as follows: the yield stress $\sigma_0 = 318$ MPa, the tensile strength $R_m = 446$ MPa, and the displacement percentage $A_5 = 33.9\%$. According to the strength curves $\sigma(\varepsilon)$ obtained, the nominal normal stress σ versus the longitudinal strain ε was determined for S235JR steel.

The elastic-plastic properties of S235JR steel was described by the tensile strength curve (Fig. 4) according to approximation model proposed by KOSSAKOWSKI [19]:

$$(4.1) \qquad \begin{aligned} \varepsilon &= \frac{\sigma}{E} & \text{for} \quad \sigma < \sigma_0 \\[2mm] \varepsilon &= \frac{\varepsilon_1 - \varepsilon_0}{\sigma_1 - \sigma_0}(\sigma - \sigma_0) + \varepsilon_0 & \text{for} \quad \sigma_0 \le \sigma \le \sigma_1 \\[2mm] \varepsilon &= \varepsilon_0 + \frac{\sigma_{01}}{E} \left(\frac{\sigma}{\sigma_{01}} \right)^{1/N} & \text{for} \quad \sigma > \sigma_1 \end{aligned}$$

where: ε – strain, ε_0 – yield strain, ε_1 – initial hardening strain, σ – stress, σ_0 – yield stress, σ_1 – initial hardening stress, σ_{01} – initial stress at the beginning of nonlinear part of approximation curve, E – modulus of elasticity, N – strain-hardening exponent.

As mentioned before, the initial porosity for tested material was determined during the microstructural examinations. The average value of initial void volume fraction was assumed, i.e. $f_0 = 0.001$ for S235JR steel.

Basing on the results obtained by FALESKOG et al. [21], TVERGAARD's parameters were determined. For the ratio $\sigma_0/E = 0.00155$ and strain-hardening exponent $N = 0.195$, their values were established as $q_1 = 1.91$, $q_2 = 0.79$ and $q_3 = 3.65$.
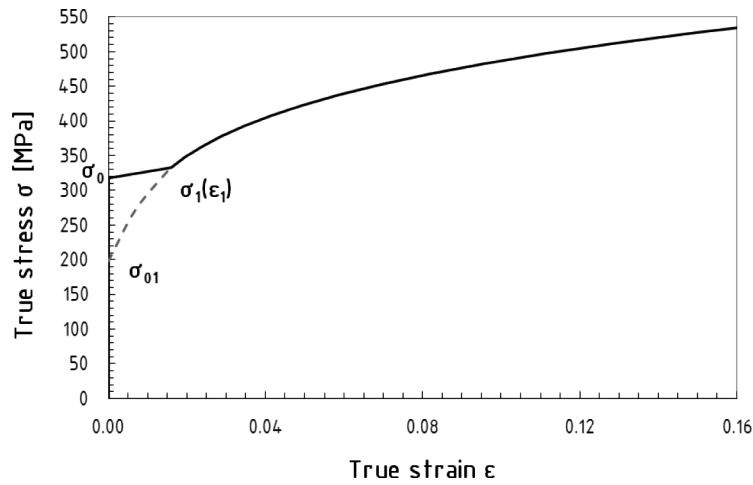
Fig. 4. Approximation true stress-strain $\sigma(\varepsilon)$ curve for S235JR steel.

Table 1

The strength parameters for S235JR steel [19].

ε_0	ε_1	σ_0 [MPa]	σ_{01} [MPa]	σ_1 [MPa]	E [GPa]	N
0.002	0.015	318	198	333	205	0.195

Other GTN material parameters for S235JR steel were determined by numerical modelling of tensile strength tests. A program based on the Finite Element Method, Abaqus Explicit version 6.10 was applied. The elements were modelled as axially symmetrical components using standard elements [22].

Basing on the $\sigma(\varepsilon)$ curves obtained through numerical analysis and experiments, the other GTN parameters were determined. They were changed within certain limits iteratively using the optimization criterion based on the convergence of the $\sigma(\varepsilon)$ values obtained numerically and experimentally.

The critical void volume fraction f_c was determined as $f_c = 0.06$, taking into account results obtained by RICHELSEN and TVERGAARD [23]. In order to analyse whole failure range, the critical void volume fraction corresponding to the complete loss of material strength was assumed as $f_F = 0.667$. The volume fraction of the nucleated voids was $f_N = 0.04$, the average nucleation strain was $\varepsilon_N = 0.30$, and the standard deviation of the strain was $s_N = 0.05$. All GTN parameters for S235JR steel are summarized in Table 2.

The nominal stress-strain $\sigma(\varepsilon)$ curves for S235JR steel determined during experiments and numerical simulations are presented in Figure 5.

Experimental input data collected in [19].

f_0	f_c	f_F	q_1	q_2	q_3	ε_N	f_N	s_N
0.0000 0.0010 0.0024	0.06	0.667	1.91	0.79	3.65	0.3	0.04	0.05
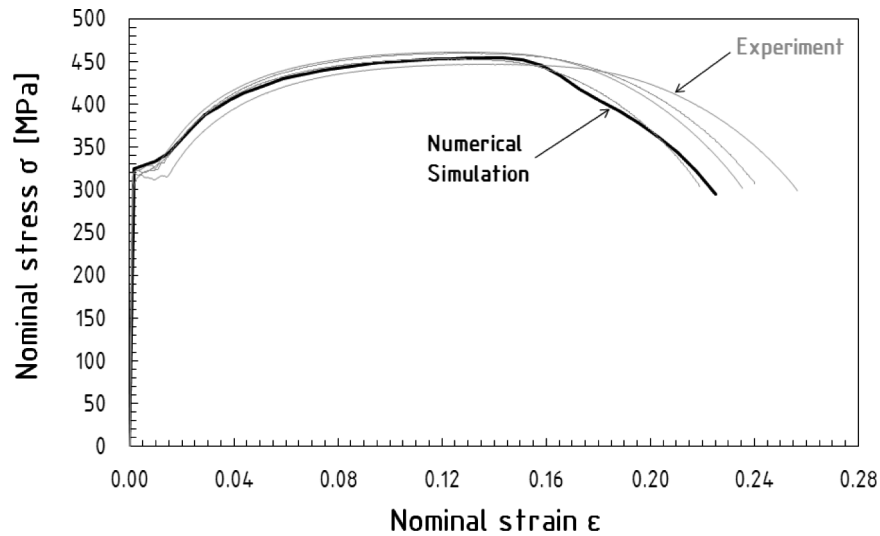
Fig. 5. Nominal stress-strain $\sigma(\varepsilon)$ curves for S235JR steel.

5. INFLUENCE OF INITIAL VOID VOLUME FRACTION f_0 ON STRENGTH PROPERTIES OF S235JR STEEL

The influence of initial void volume fraction on the strength properties of S235JR steel was examined by numerical simulations of tensile tests of specimens with a circular cross-section described before. The elements were analysed using Abaqus version 6.10 program and Dynamic Explicit module.

The specimens were subjected to quasi-static tension under displacement control increase. The axially symmetrical elements were applied. Because of the symmetry, only half-specimens were considered. In the middle of the sample length a sharp notch with a depth of $R = 0.05$ mm was modelled (Fig. 6).

As mentioned before, during numerical simulations with the finite element method, especially when GTN model is used, the mesh-size effect is encountered. It reveals the softening of the final part of the strength curve. During the numerical simulations performed, two assumptions were applied in order to check the influen-
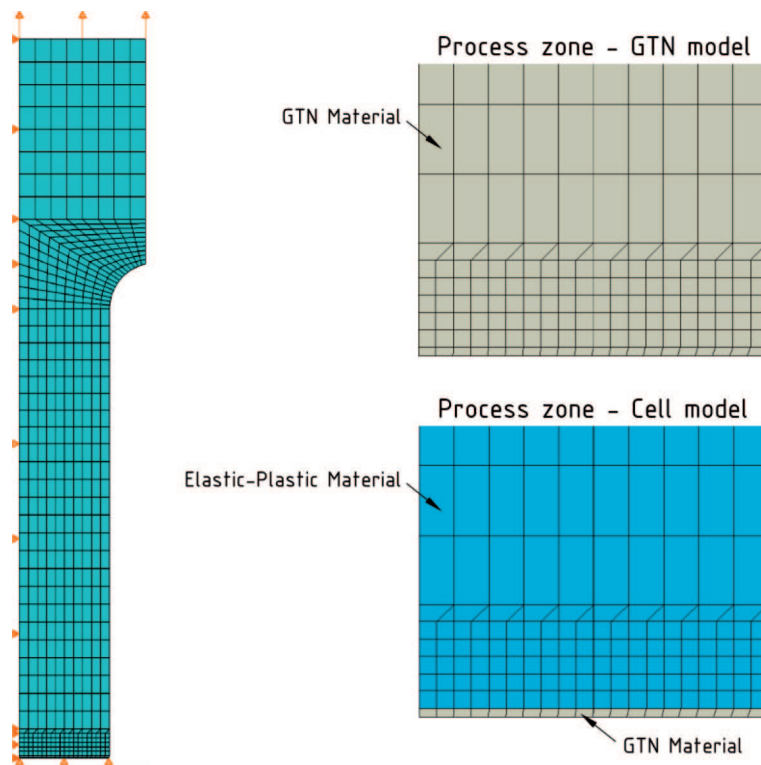
Fig. 6. Scheme of numerical models and process zone.

ce of the modelling method to minimize the mesh size effect. In the first case, the GURSON-TVERGAARD-NEEDLEMAN material model for porous solids was assumed for the whole numerical model. This model is referred as *GTN model*. In the second model, referred as *Cell model*, only the elements near the crack plane were modelled with using the GTN material model. The elastic-plastic material model was assumed for the rest of the numerical model (Fig. 6).

Both of the models were based on the microstructurally-based length scales methods, whose principle is given below. In order to form a macroscopic crack, the fracture criterion must be satisfied over a minimum volume of material, defined in two dimensions by a characteristic length measure l_c in the region of high stresses and plastic strain. Although several approaches have been discussed, the length scale determination is still subjective. The approach based on HANCOCK's and MACKENZIE's method [24] was used in presented study. According to this, the fracture is due to linking of two or more holes formed from coalescing inclusion colonies. The macro-crack formation only occurs when shear localizes between multiple clusters, while void growth expands the cluster of inclusion colonies. The length scale is represented by the size of these inclusion colonies, which are visible in a fractograph.

In presented study the characteristic length l_c was defined as the dimensions of plateaus and valleys measured on the fracture surface and the results of analysis performed before were used [19]. The statistical CHAUVENET's criterion was used during measurements for twenty inclusion colonies analysed, rejecting all atypical values. The characteristic length l_c ranged from 130 μm to 360 μm. The the mean value of l_c was determined as $l_c \approx 250$ μm.

The dimensions of the mesh in the area close to the fracture plane, i.e. *process zone*, were equal to $D \times D/2$, where D was equal to the characteristic length $l_c = 250$ μm determined during microstructural examinations. The scheme of numerical models and process zone are presented in Figure 6.

The analysis of the influence of the initial void volume fraction on the strength properties of S235JR was based on the force-elongation $F(l)$ curves determined during experiments and numerical simulations.

As mentioned before, three values of initial void volume fraction of S235JR was considered, $f_0 = 0$, $f_0 = 0.001$ and $f_0 = 0.0024$.

The force-elongation curves $F(l)$ determined during experiments and numerical simulations by using *GTN* and *Cell models* are shown in Figures 7 and 8.

The tensile strength curves obtained by applying both *GTN* and *Cell model* were consistent with the experimental results in the first range, until the maximum force F was reached. The differences revealed in the next range, from the maximum force F to the failure.
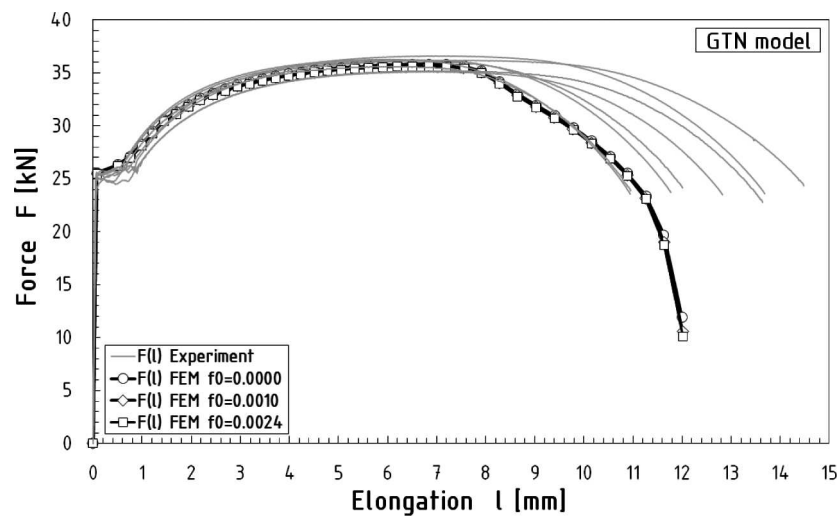

Fig. 7. Force-elongation $F(l)$ curves determined during experiments and numerical simulations by using *GTN model* for different values of f_0.

When *GTN model* was used, the visible softening was noticed. A sharp decrease in force was observed, after the maximum force was reached, corresponding to elongation

equal to ~8.0 mm. After that point, the forces F determined during the experiments were higher than those calculated during numerical simulations.

The simulated failure of the elements for *GTN model* was noticed in the range of elongation equal to 11.2-11.7 mm.

Better agreement of the results obtained experimentally and numerically was noticed when *Cell model* was applied for whole range of strength curves. The simulated failure of elements was noticed for elongation equal to 11.5-11.7 mm.
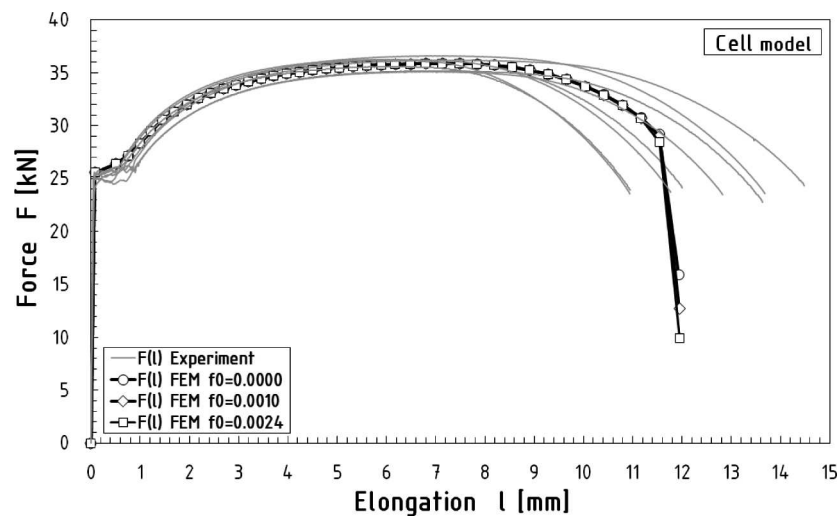

Fig. 8. Force-elongation $F(l)$ curves determined during experiments and numerical simulations by using *Cell model* for different values of f_0.

Overall, the strength curves obtained numerically by assuming all three initial void volume fractions f_0 were similar for both *GTN* and *Cell models* applied. The highest values of forces were noticed when the fully dense material without pores was considered, i.e. $f_0 = 0$, while the lowest values of forces were for maximum porosity, i.e. $f_0 = 0.0024$.

The insignificant differences in values of forces were recorded in the first range, for elongation from $l = 0$ up to $l = 11.2$ mm for *GTN model*. They ranged from 0.24% for $f_0 = 0$ and $f_0 = 0.001$ up to 0.90% for $f_0 = 0$ and $f_0 = 0.0024$. For the failure range, above elongation $l = 11.2$ mm, the differences were higher, from 2.11% for $f_0 = 0$ and $f_0 = 0.001$ up to 18.37% for $f_0 = 0$ and $f_0 = 0.0024$.

When *Cell model* was applied, the values of forces in the first range were the same for all initial void volume fractions f_0 assumed. The significant differences were noticed in the failure range, for elongation above $l = 11.5$ mm, from 0.67% for $f_0 = 0$ and $f_0 = 0.001$ up to 2.44% for $f_0 = 0$ and $f_0 = 0.0024$.

Assuming two general situations, the fully dense material without pores and the maximum porosity for S235JR steel reveals in slight differences in the void volume fraction of the material.

Analysing the obtained values of *VVF* it should be noted that they are generally higher in the middle of the element in comparison to the external part of the area near the fracture plane. Therefore, the initiation of fracture is expected in the middle of the sample. The void volume fraction *VVF* curves shown in Figures 9 and 10 are presented for point in the middle of the fracture plane, on the axis of the sample.
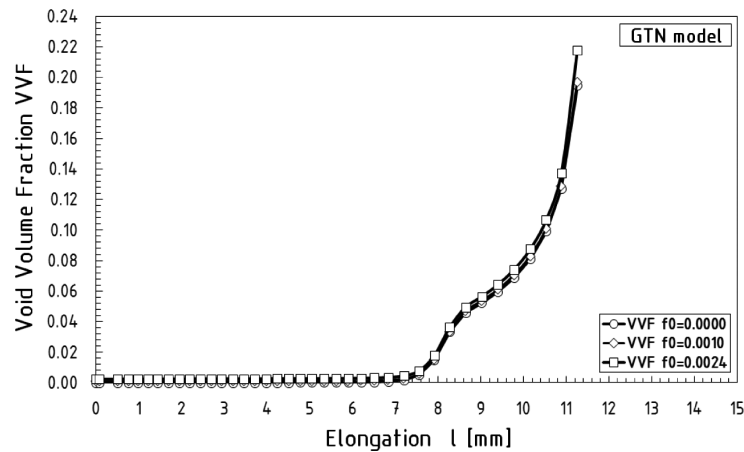

Fig. 9. Void Volume Fraction *VVF* curves determined during numerical simulations by using *GTN model* for different values of f_0.
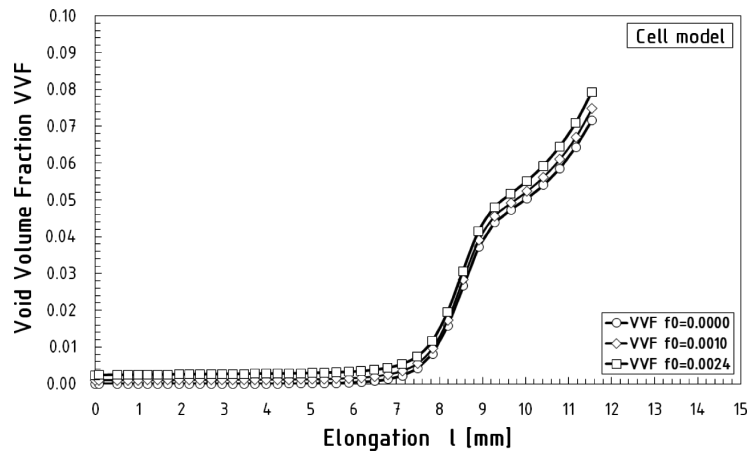

Fig. 10. Void Volume Fraction *VVF* curves determined during numerical simulations by using *Cell model* for different values of f_0.

As can be seen in Figures 9 and 10, the beginning of the increase in the void volume fraction *VVF* was similar for all initial void volume fraction f_0 assumed for both numerical models applied.

When *GTN model* was used, the voids increased for elongation above $l = 7.0$ mm. The voids increased much rapidly at final, failure range, for $l > 11.2$ mm. The maximum difference 11.87% in void volume fraction was noticed for $f_0 = 0$ and $f_0 = 0.0024$ assumed.

For *Cell model* the increase of the void volume fraction was observed for elongation above $l = 7.0$ mm, similarly to *GTN model*. In the next range, the voids increased less in comparison to *GTN model*. At the final part, the void volume fraction differed maximum 10.75% for $f_0 = 0$ and $f_0 = 0.0024$ assumed.

6. DISCUSSION

Analysing the results obtained, the several key phenomena were observed.

For the first, the influence of initial porosity on the strength of S235JR steel was slight. This phenomenon was observed for all three initial void volume fractions f_0 assumed, i.e. two general situations, for fully dense material without pores and its maximum porosity. The highest and the lowest strength of the material was observed when the fully dense material without pores was considered, i.e. $f_0 = 0$, and maximum porosity was assumed, i.e. $f_0 = 0.0024$, respectively.

This phenomenon allows to assume the average values of initial void volume fraction f_0 for S235JR steel in a common engineering calculations. In order to obtain more conservative results, the maximum values of $f_0 = 0.0024$ is recommended. However, the similar results should be expected for such assumed f_0 for both *GTN* and *Cell* numerical models. The strength curves determined numerically for *GTN* and *Cell models* assuming the average porosity, i.e. $f_0 = 0.001$ for S235JR steel are presented in Figure 11. As can be seen, the softening phenomenon described before is clearly visible when *GTN model* is applied in opposition to *Cell model*.

The current void volume fraction increase is the next considered issue. For both *GTN* and *Cell models* used, the values of *VVF* are similar in the first range, from the beginning up to the maximum force, corresponding to elongation about $l = 7.0$ mm. The voids begin to grow intensively for $l > 7.0$ mm, but their increase is more rapid when *GTN model* is used in comparison to *Cell model*. The critical values of the void volume fraction determined at the moment of expected failure are 0.197 and 0.075, for *GTN* and *Cell model* respectively.

The phenomenon described above was observed for other values of initial void volume fraction, i.e. $f_0 = 0$ and $f_0 = 0.0024$, and was closely related to numerical model assumed. As it was presented in previous research performed by KOSSAKOWSKI [19], when *GTN model* was used, the observed increase of the porosity leads to significant reduction of the strength through the assuming the voided material for the
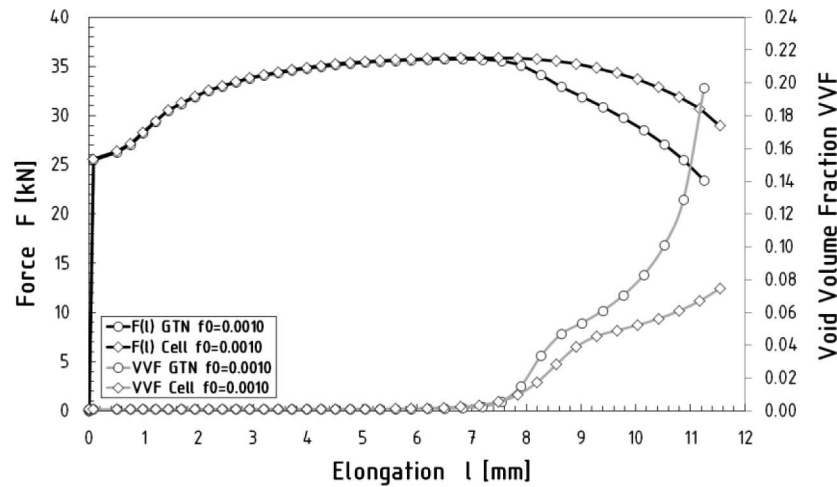
Fig. 11. Force-elongation $F(l)$ and Void Volume Fraction VVF curves determined numerically by using *GTN* and *Cell models* for $f_0 = 0.001$.

entire numerical model. In the case when *Cell model* is applied, the *process zone* is modelled as a layer of material containing a pre-existing population of similar sized voids, containing a single void of some initial volume f_0. It leads to smooth reduction of material strength, revealing the lower increase in porosity in the material.

7. Conclusions

Based on the results of the analysis performed, the following conclusions have been drawn:
1. The tensile strength curves obtained by applying *GTN model* were consistent with the experimental results in the first range, until the maximum force F was reached. The visible softening was noticed in the next range, from the maximum force up to the failure. Good agreement of results was noticed for whole range of strength curves when *Cell model* was applied.
2. Overall, the strength curves obtained numerically by assuming all three initial void volume fractions f_0 were similar for both *GTN* and *Cell models* applied. It can be noticed, that considered porosity of S235JR steel has a low influence on its strength at low stress triaxiality. The highest values of force were noticed when the fully dense material without pores was considered, i.e. $f_0 = 0$, while the lowest values of force were observed for maximum porosity, i.e. $f_0 = 0.0024$.
3. Assuming two general situations, the fully dense material without pores and the maximum porosity for S235JR steel revealed in slight differences of the void volume fraction of the material.

4. The beginning of the increase in the void volume fraction was similar for all assumed values of f_0 for both numerical models applied. Voids started to increase for elongation corresponding to the maximum force. Their growth was much rapid at final, failure range, especially for *GTN model* applied.

5. Taking into consideration the results obtained, the average values of initial void volume fraction $f_0 = 0.001$ for S235JR steel is recommended to use in common engineering calculations for elements operating at low stress triaxiality. In order to obtain more conservative results, the maximum values of $f_0 = 0.0024$ may be used.

References

1. D. Teirlinck, F. Zok, J.D. Embury, M.F. Ashby, *Fracture Mechanism Maps in Stress Space*, Acta Metallurgica' **36**, 5, 1213-1228, 1988.

2. A.L. Gurson, *Continuum Theory of Ductile Rupture by Void Nucleation and Growth: Part I – Yield Criteria and Flow Rules for Porous Ductile Media*, Journal of Engineering Materials and Technology, Transactions of the ASME, **99**, 1, 2-15, 1977.

3. V. Tvergaard, *Influence of Voids on Shear Band Instabilities under Plane Strain Conditions*, International Journal of Fracture, **17**, 4, 389-407, 1981.

4. V. Tvergaard, A. Needleman, *Analysis of the Cup-Cone Fracture in a Round Tensile Bar*, Acta Metallurgica, **32**, 1, 157-169, 1984.

5. PN-EN 1993-1-10:2007 Eurocode 3: Design of Steel Structures - Part 1-10: Material Toughness and Through-thickness Properties.

6. G. Sedlacek, M. Feldmann, B. Kühn, D. Tschickardt, S. Höhler, C. Müller, W. Hensen, N. Stranghöner, W. Dahl, P. Langenberg, S. Münstermann, J. Brozetti, J. Raoul, R. Pope, F. Bijlaard, *Commentary and Worked Examples to EN 1993-1-10 "Material toughness and through thickness properties" and other toughness oriented rules in EN 1993*, JRC Scientific and Technical Reports, European Commission Joint Research Centre, 2008.

7. P.G. Kossakowski, *An Analysis of the Load-Carrying Capacity of Elements Subjected to Complex Stress States with a Focus on the Microstructural Failure*, Archives of Civil and Mechanical Engineering **10**, 2, 15-39, 2010.

8. P.G. Kossakowski, W. Trąmpczyński, *Numerical simulation of S235JR steel failure with consideration of the influence of microstructural damages* [in Polish], Przegląd Mechaniczny 4, 15-22, 2011.

9. K. Nahshon, J.W. Hutchinson, *Modification of the Gurson Model for shear failure*, European Journal of Mechanics – A/Solids, **27**, 1, 1-17, 2008.

10. A. Biegus, D. Czepiżak, *Experimental and numerical studies upon load-bearing capacity of locally strengthened corrugated sheets*, Archives of Civil Engineering, **55**, 1, 11-28, 2009.

11. A. Biegus, D. Czepiżak, *Evaluation of resistance of corrugated sheets under bending by a concentrated loads from the local suspensions*, Archives of Civil Engineering, **56**, 4, 283-297, 2010.

12. P. Iwicki, *Sensitivity analysis of buckling loads of bisymmetric i-section columns with bracing elements*, Archives of Civil Engineering, **56**, 1, 69-88, 2010.

13. U. Radoń, *Analysis of reliability and stability of bar structures*, Archives of Civil Engineering, **56**, 2, 155-172, 2010.

14. M. Kamiński, P. Swita, *Reliability modeling in some elastic stability problems via the generalized stochastic finite element method*, Archives of Civil Engineering, **57**, 3, 275-295, 2011.

15. J. Chrościelewski, M. Rucka, K. Wilde, W. Witkowski, *Formulation of spectral truss element for guided waves damage detection in spatial steel trusses*, Archives of Civil Engineering, **55**, 1, 43-63, 2009.

16. W. Witkowski, M. Rucka, K. Wilde, J. Chrościelewski, *Wave propagation analysis in spatial frames using spectral timoshenko beam elements in the context of damage detection*, Archives of Civil Engineering, **55**, 3, 367-402, 2009.

17. A.G. Franklin, *Comparison between a quantitative microscope and chemical method for assessment on non-metallic inclusions*, Journal of the Iron and Steel Institute, 207, 181-186, 1969.

18. PN-EN 10025-1:2005 Hot Rolled Products of Structural Steels -– Part1: General Technical Delivery Conditions.

19. P.G. Kossakowski, *Simulation of ductile fracture of S235JR steel using computational cells with microstructurally-based length scales*, Journal of Theoretical and Applied Mechanics, **50**, 2, 589-607, 2012.

20. PN-EN 10002-1:2004 Metallic Materials – Tensile Testing – Part 1: Method of Test at Ambient Temperature.

21. J. Faleskog, X. Gao, C.F. Shih, *Cell model for nonlinear fracture analysis – I. Micromechanics calibration*, International Journal of Fracture, **89**, 4, 355-373, 1998.

22. Abaqus 6.10 Analysis User's Manual, Dassault Systèmes, 2010.

23. A.B. Richelsen, V. Tvergaard, *Dilatant Plasticity or Upper Bound Estimates for Porous Ductile Solids*, Acta Metallurgica et Materialia, **42**, 8, 2561-2577, 1994.

24. J.W. Hancock, A.C. Mackenzie, *On the mechanisms of ductile failure in high-strength steels subjected to multi-axial stress-states*, Journal of Mechanics and Physics of Solids, **24**, 2-3, 147-160, 1976.